Letter

Trions in MoS_2 are quantum superpositions of intra- and intervalley spin states

J. Klein,[1,2,*] M. Florian,[3,4] A. Hötger,[1] A. Steinhoff,[3] A. Delhomme,[5] T. Taniguchi,[6] K. Watanabe,[7] F. Jahnke,[3] A. W. Holleitner,[1] M. Potemski,[5] C. Faugeras,[5] A. V. Stier,[1,†] and J. J. Finley[1,‡]

[1]*Walter Schottky Institut and Physik Department, Technische Universität München, Am Coulombwall 4, 85748 Garching, Germany*
[2]*Department of Materials Science and Engineering, Massachusetts Institute of Technology, Cambridge, Massachusetts 02139, USA*
[3]*Institut für Theoretische Physik, Universität Bremen, P.O. Box 330 440, 28334 Bremen, Germany*
[4]*Department of Electrical Engineering and Computer Science, University of Michigan, Ann Arbor, 48109 Michigan, USA*
[5]*Université Grenoble Alpes, INSA Toulouse, Université Toulouse Paul Sabatier, EMFL, CNRS, LNCMI, 38000 Grenoble, France*
[6]*International Center for Materials Nanoarchitectonics, National Institute for Materials Science, 1-1 Namiki, Tsukuba 305-0044, Japan*
[7]*Research Center for Functional Materials, National Institute for Materials Science, 1-1 Namiki, Tsukuba 305-0044, Japan*

(Received 16 January 2021; revised 22 December 2021; accepted 11 January 2022; published 31 January 2022)

We report magnetophotoluminescence spectroscopy of gated MoS_2 monolayers in high magnetic fields to 28 T. At $B = 0$ T and electron density $n_s \sim 10^{12}$ cm^{-2}, we observe three trion resonances that cannot be explained within a single-particle picture. Employing *ab initio* calculations that take into account three-particle correlation effects as well as local and nonlocal electron-hole exchange interaction, we identify those features as quantum superpositions of *inter*- and *intravalley* spin states. We experimentally investigate the mixed character of the trion wave function via the filling factor dependent valley Zeeman shift in positive and negative magnetic fields. Our results highlight the importance of exchange interactions for exciton physics in monolayer MoS_2 and provide insights into the microscopic understanding of trion physics in two-dimensional multivalley semiconductors for low excess carrier densities.

DOI: 10.1103/PhysRevB.105.L041302

Early experiments on quasi-two-dimensional CdTe [1] and GaAs [2–4] quantum wells allowed the observation of charged exciton complexes owing to an increase in the exciton binding energy arising from confinement effects. Atomically thin transition metal dichalcogenides (TMDCs) of formula MX_2 where $M =$ Mo, W and $X =$ S, Se, or Te are excellent model systems for studying excitonic physics in two-dimensional (2D) systems, due to enhanced quantum confinement and weak dielectric screening [5–9]. The inherent 2D nature, broken spatial inversion symmetry, and strong spin-valley optical selection rules [10] open up a plethora of possibilities for the controlled study of exciton physics in the presence of free carriers [11–15]. Combined with the ability to integrate monolayers into functional devices, such experiments can be performed with full control of the local charge density. Unlike quasi-2D quantum well systems, valley dichroism and strong spin-orbit splitting in the conduction and valence bands promotes the formation of dipole allowed trion complexes having singlet and triplet spin structure [16–22]. In WSe_2 and WS_2, the lowest energy exciton is spin forbidden due to a dark band alignment arising from the large conduction band spin-orbit splitting of $\Delta_{CB} \sim 30$ meV [23–27]. This is in stark contrast to $MoSe_2$ [12], a material that is considered to be optically bright since the lowest exciton transition is spin allowed [22,23,25,28,29].

The situation for MoS_2 is, however, more delicate. Initial experiments showed an increase of exciton luminescence intensity with temperature [30,31], which is a clear signature for an optically bright material, supporting early theoretical works [23,32]. However, unlike optically bright $MoSe_2$, monolayer MoS_2 shows a large degree of valley polarization that is typically found in the optically dark materials, like WSe_2 and WS_2. Importantly, recent experiments on magnetic brightening of dark excitons unequivocally showed an optically dark alignment with a splitting between $1s$ states of bright and dark excitons of $\Delta_{db} \sim 14$ meV [29], which is consistent with more recent theoretical work [33–36]. This value reflects both the SOC in the conduction band and the difference in the effective mass of the two subbands, which leads to the inversion of the ground state between the single-particle and excitonic picture. As such, the single-particle conduction band structure of MoS_2 is nontrivial due to the small spin splitting and it is altered by interactions in the exciton picture [see Figs. 1(a) and 1(b)]. Furthermore, a hallmark of optically dark materials is the appearance of a rich fine structure of excitonic complexes [37,38] as recently observed experimentally [22,39,40]. However, these initial experiments lacked a gate to control the local charge carrier density and a fully developed microscopic understanding of the observed spectra. This motivates detailed charge-carrier-dependent investigations of the trion fine structure in monolayer MoS_2. In this Letter, we show that the local and nonlocal exchange interactions (U_{eh}) determine the band alignment and corresponding trion fine structure in monolayer MoS_2. We further calculate how the mixing of unperturbed *inter*/*intravalley* trion states is driven

*jpklein@mit.edu
†andreas.stier@wsi.tum.de
‡finley@wsi.tum.de

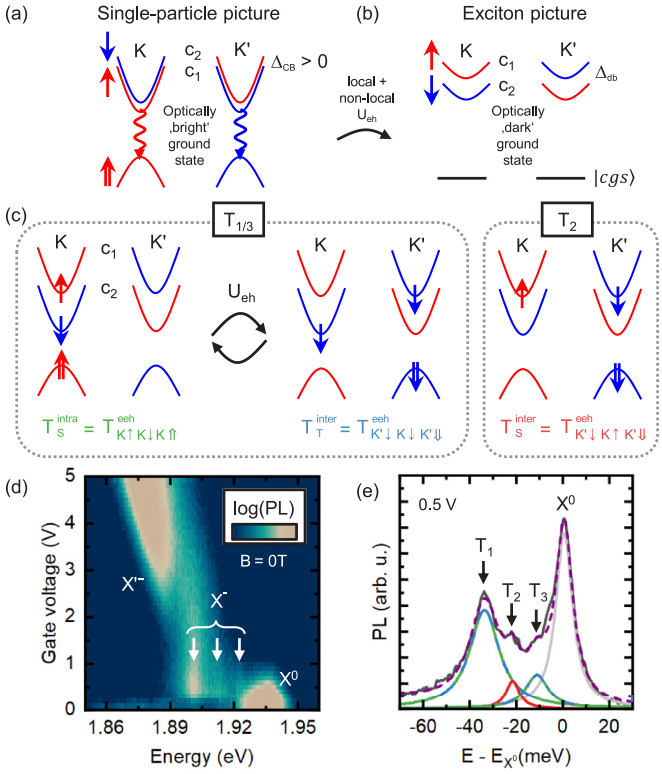

FIG. 1. (a) Monolayer MoS_2 is optically bright in a single-particle picture with $\Delta_{CB} > 0$. (b) Local exchange interaction U_{eh} reorders exciton spin configurations resulting in the lowest transition to be optically dark. This is schematically depicted as a flip of conduction bands. (c) Trion fine structure in monolayer MoS_2: Three bright configurations are given by the intravalley singlet $T_S^{\text{intra}} = T^{eeh}_{K\uparrow K\downarrow K\Uparrow}$ (left) and intervalley triplet trion $T_T^{\text{inter}} = T^{eeh}_{K'\downarrow K\downarrow K'\Downarrow}$ (center), which are coupled by nonlocal electron-hole exchange interaction U_{eh}, as well as the intervalley singlet trion $T_S^{\text{inter}} = T^{eeh}_{K'\downarrow K\uparrow K'\Downarrow}$ (right). The trion amplitude denoted by $T^{e_1e_2h_3}_{\mathbf{k_1}\mathbf{k_2}\mathbf{k_3}} = \langle (a^{e_2}_{\mathbf{k_1}+\mathbf{k_2}+\mathbf{k_3}})^\dagger a^{h_3}_{\mathbf{k}_3} a^{e_2}_{\mathbf{k}_2} a^{e_1}_{\mathbf{k}_1} \rangle$ is a four-operator expectation value and describes the correlated process of annihilating two electrons and one hole, leaving behind an electron with momentum $\mathbf{Q} = \mathbf{k_1} + \mathbf{k_2} + \mathbf{k_3}$ in the conduction band, and is linked to the optical response of an electron trion. We adopt the band ordering from the exciton picture. (d) False color plot of the gate voltage dependent 5-K PL showing the neutral exciton X^0 and a fine structure of negatively charged trions X^- (highlighted with arrows) and a many-body state X'^- at 2 V (densities of $n_s > 4 \times 10^{12}$ / cm^2) (e) Fitted PL spectrum at 0.5 V ($n_s \sim 10^{12}$) cm^{-2} showing three distinct trion resonances T_1, T_2, and T_3 with binding energies of -33.7, -21.5, and -10.8 meV.

by the exchange interactions and therefore modify the binding energies and wave function contributions of the observed trion features. This has strong implications for the interpretation of magneto-optical data in many works on 2D multivalley semiconductors [8,24,39,41–52].

The band structure of monolayer MoS_2 deviates from other semiconducting TMDCs due to the small conduction band splitting in the single-particle picture. While the ground state is optically bright [see Fig. 1(a)], small many-body effects can markedly alter the band structure [53,54]. Local electron-hole exchange interaction leads to an overall blueshift of like-spin excitons that reorders excitonic transitions and results in an optically dark ground state [see Fig. 1(b) and the Supplemental Material [55] for calculations on the trion spectra, which includes Refs. [16,32,37,38,56–63]]. In addition, nonlocal electron-hole exchange mixes excitons in the K and K' valleys, resulting in a nonanalytic lightlike exciton dispersion for like-spin excitons. A detailed discussion for monolayer MoS_2 is given in Ref. [37].

Furthermore, these interactions result in three trion configurations [Fig. 1(c)], which are quantum superpositions of the eigenstates of the three-body problem without electron-hole exchange interaction: an intravalley singlet $T_S^{\text{intra}} = T^{eeh}_{K\uparrow K\downarrow K\Uparrow}$ and an intervalley triplet trion $T_T^{\text{inter}} = T^{eeh}_{K'\downarrow K\downarrow K'\Downarrow}$ that are coupled due to nonlocal electron-hole exchange interaction U_{eh} as well as an intervalley singlet trion $T_S^{\text{inter}} = T^{eeh}_{K'\downarrow K\uparrow K'\Downarrow}$ where both electrons are located in the upper conduction bands c_1. Under applied magnetic fields in the range $B = \pm 28$ T, we observe quantum oscillations in the intensity of the dominant trion emission line and observe that the polarity of the magnetic field switches the PL between intravalley singlet and intervalley triplet character due to time-reversal symmetry breaking and Landau level (LL) quantization. From our data we draw two main conclusions: (i) Trions observed in optical spectra have mixed wave function character, thus representing quantum superpositions with contributions from intravalley and intervalley singlet and triplet trions, and (ii) the nonuniform and tunable trion g factor results from the decay of the trion into a photon and a free electron sequentially occupying Landau levels in the K and K' conduction bands.

We probe trion emission from an exfoliated monolayer MoS_2 in a commonly used gate-tunable van der Waals device structure (see the Supplemental Material [55] for additional information on the device, which includes [53,64–69]) [15]. The monolayer MoS_2 is fully encapsulated between thin layers of hBN (∼10 nm) to reduce inhomogeneous linewidth broadening [47,65]. We apply a bias voltage between MoS_2 and a thin graphite bottom gate to control the carrier concentration n_s in the device [53]. Low-temperature 5-K magnetophotoluminescence measurements were performed using unpolarized cw laser excitation at $E = 2.41$ eV and σ^- circularly polarized detection. A typical false color plot of gate voltage dependent photoluminescence (PL) obtained from our device is presented in Fig. 1(d) and Fig. SM1 of the Supplemental Material [55]. At zero carrier density, the PL is dominated by the neutral exciton X^0, as expected. When the electron density is increased, the oscillator strength shifts away from X^0 due to the formation of negatively charged excitons before spectral weight transitions to a many-body state X'^- at >2 V (densities $n_s > 4 \times 10^{12}$ cm^{-2}) [14,53,54]. Interestingly, besides the neutral exciton X^0 close to $n_s = 0$, three distinct trion resonances, T_1, T_2, and T_3 are clearly visible for a gate voltage of 0.5 V (electron density of $n_s \sim 1 \times 10^{12}$ cm^{-2}) further highlighted by the fit in Fig. 1(e). The voltage dependent oscillator strength due to band population of the individual trions is nontrivial due to the delicate interplay between the single-particle and exciton picture in which the conduction band configuration reorders due to nonlocal exchange interaction. In order to explain the threefold trion fine structure, we numerically solve a generalized three-particle Schrödinger equation to determine resonances in the optical absorption of hBN encapsulated monolayer MoS_2 at

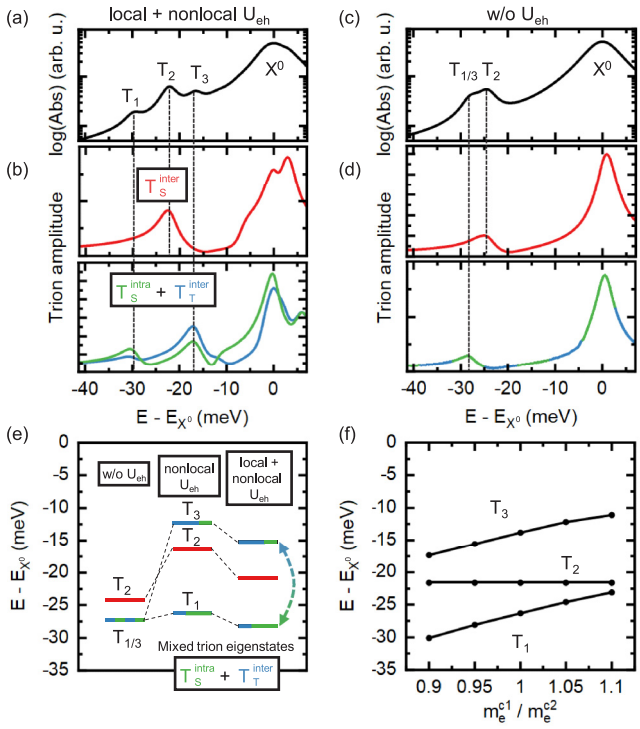

FIG. 2. (a) Calculated absorption spectrum of hBN encapsulated monolayer MoS_2 with and (c) without electron-hole exchange interaction U_{eh} for a carrier density of $n_s = 0.1 \times 10^{12}$ cm^{-2}. A phenomenological homogeneous broadening of 4 meV (full width at half maximum) has been used. (b),(d) Corresponding wave function contributions from the T_S^{inter}, T_S^{intra}, and T_T^{inter} of the trion configurations to the absorption spectrum of hBN encapsulated monolayer MoS_2. Note that only wave function contributions for $\mathbf{Q} = \mathbf{K}/\mathbf{K}'$ are shown. As a result, the exciton-electron scattering states in the high-energy tail of the exciton [59] are only coarsely sampled, which results in an artificial splitting of the exciton. (e) Calculated binding energies ($E - E_{X^0}$) of trion resonances, without U_{eh}, only with nonlocal U_{eh} and with both local and nonlocal U_{eh}. The latter forms quantum superpositions by strongly admixing the trion eigenstates T_S^{intra} and T_T^{inter} shown in (a). (f) Binding energies of trions T_1, T_2, and T_3 as a function of the ratio between effective electron mass of upper and lower conduction band. Results are obtained using an effective mass model for the band structure around the K/K' points of the two lowest conduction (highest valence) bands.

low carrier concentration ($n_s = 0.1 \times 10^{12}$ cm^{-2}) [60]. The method used is combined with material-realistic band structures and bare, as well as screened Coulomb matrix elements on a G_0W_0 level (see the Supplemental Material). Results for the calculated optical absorption spectra are presented in Fig. 2(a) and reveal T_1, T_2, and T_3 as individual peaks. Their experimentally observed PL counterparts can be identified in Fig. 1(e). From our calculations, we can directly show that the observed features have distinct wave function contributions from the unperturbed trion configurations [see Fig. 2(b)]. For example, the lowest energy peak, T_1, contains contributions from T_S^{intra} and T_T^{inter}, with the former dominating the total wave function. The T_3 resonance is similarly admixed with the dominant wave function contribution from the intervalley triplet trion. Only T_2 is an eigenstate of the intervalley singlet trion. Note that without electron-hole exchange interaction U_{eh}, the observed trion fine structure only shows two resonances [see Fig. 2(c)] with the corresponding wave function contributions in Fig. 2(d).

Figure 2(e) shows the evolution of the calculated trion binding energies ($E - E_{X^0}$) with local and nonlocal U_{eh}. Without U_{eh}, only two energetically distinct resonances are expected, which are conventionally labeled in the literature as the inter/intravalley trions. In contrast, including electron-hole exchange interaction predicts three resonances, as observed in our experiments. The absolute and relative energies of T_1, T_2, and T_3 (-28.5, -21.0, and -15.5 meV) are in excellent agreement with our experimental findings (-33.7, -21.5, and -10.8 meV). Moreover, since electrons from both spin-orbit split conduction bands c_1 and c_2 contribute to singlet intravalley trion and Coulomb exchange split intervalley triplet trion, their corresponding binding energy sensitively depends on the ratio of the electron band masses $m_e^{c_1}/m_e^{c_2}$ [see Fig. 2(f)]. Hence, the trion fine structure contains additional information on the difference of the electron effective masses in the c_1 and c_2 conduction bands. The T_2 trion remains unaffected since both spins are located in the same conduction band.

A qualitative understanding of the trion fine structure can be obtained from a configuration model [33,34]. The homogeneous part of the equation of motion for the trion amplitude $T^{e_1e_2h_3}_{\mathbf{k}_1\mathbf{k}_2\mathbf{k}_3}$ constitutes a three-particle Hamiltonian whose eigenstates describe trions with total momentum $\mathbf{Q}$ (see the Supplemental Material for details [55]). The Hamiltonian can be split into a part H_0 without electron-hole exchange and an exchange part H_U according to the Coulomb matrix element. Configurations are eigenstates of the three-particle Hamiltonian H_0 that contains the kinetic energies of two electrons and a hole as well as the direct Coulomb interaction. There are six optically bright trion configurations in the subspace of zero-momentum trions with a hole located in the highest valence band [19]. Due to time-reversal symmetry, the configurations are pairwise degenerate and are connected by changing K into K' and flipping all spins. In Fig. 1(c) the configurations are shown for $\mathbf{Q} = \mathbf{K}$. By adding electron-hole exchange to this picture, interaction between the configurations is introduced and leads to new eigenstates and -energies. It is these new eigenstates that are observed in our experiments, rather than the unmixed configurations. Throughout the remainder of the Letter we label the most prominent trion feature T_1 as the "negative trion" X^- to directly link it to other reports in the literature.

We continue to probe the mixed character of the X^- via magneto-optical experiments in high magnetic fields in device A and an additional, second, dual-gated device B. We focus our discussion on the T_1 resonance for which we obtain statistically reliable data for both devices. Figure 3(a) shows a typical example of the PL recorded at $B = -22$ T as a function of gate voltage on device A. Clearly, the X^- PL shows gate-voltage-dependent oscillations in its intensity [side panel of Fig. 3(a)], which we can observe already at lower B (see the Supplemental Material for additional data). The peaks of these quantum oscillations are attributed to half filling of LLs with filling factors $\nu = +0$ and $\nu = +1$ [51]. As detailed in

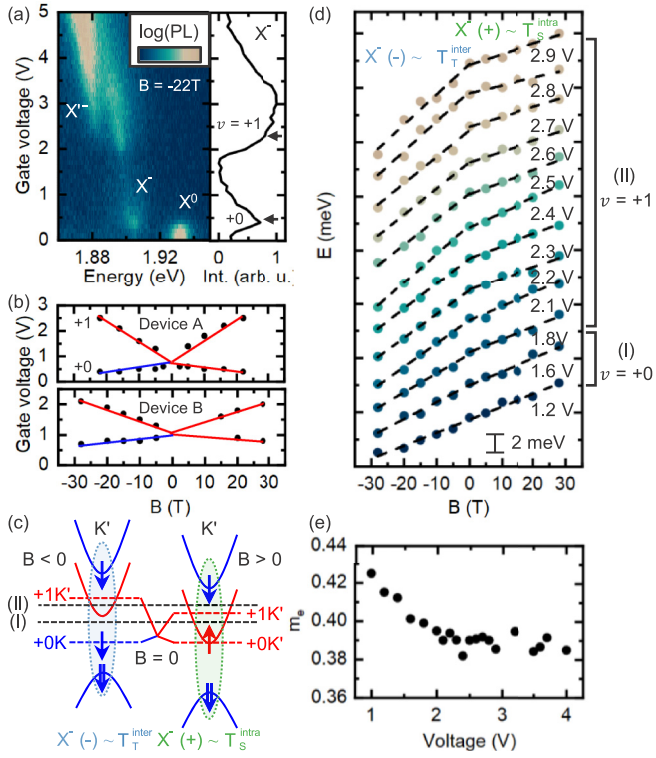

FIG. 3. (a) Left panel: Electron density dependent μ-PL at $B = -22$ T of device A. Right panel: Corresponding integrated X^- intensity. The X^- reveals LL quantization as indicated by the dashed lines with filling factor $\nu = +0$ and $\nu = +1$. (b) LL fan diagram of devices A and B. Solid lines serve as a guide to the eye. The blue (red) color of the LLs corresponds to spin $\uparrow$ (spin $\downarrow$) of the electron for the magnetic field polarity due to time reversal symmetry breaking. (c) Band configuration including the relevant LLs in the lower conduction band of the intervalley triplet trion T_T^{inter} for negative ($-$) and intravalley singlet trion T_S^{intra} for positive ($+$) magnetic field. Regime I: Only the LL with filling factor $\nu = +0$ is filled in the K (K') valley for negative (positive) magnetic field. Regime II: For negative field LL $\nu = +0$ is populated in K while $\nu = +0$ and $\nu = +1$ are in K' for positive magnetic fields. (d) X^- valley Zeeman shift in a second device B. The effective g factor for negative magnetic field increases due to LL population effects. (e) Voltage dependent electron mass m_e.

the SM and plotted in Fig. 3(b), the positions of the peaks shift linearly with B, a general observation in both investigated devices. For low electron densities, we observe that the peak emission associated with the $\nu = +0$ LL shifts downwards in gate voltage (= energy) with increasing magnetic field strength. We explain this observation by the unique features of LLs in monolayer TMDCs [70]. First, at finite magnetic field, all LLs in each respective K/K' valley are fully spin and valley polarized. As a consequence, X^- decays into a circularly polarized photon, the helicity of which depends on the K/K' valley, and an electron in a fully spin and valley polarized Landau level [see Fig. 3(c)] [24,51,70]. Uniquely, the K/K' position and, therefore, spin of the $\nu = +0$ LL depends on the polarity of the applied magnetic field, being either spin $\downarrow$ at $B < 0$ or spin $\uparrow$ at $B > 0$. In other words, both valley index and spin of the 0th Landau level in the conduction band flip depending on the polarity of B. Since we only detect σ^- PL in our experiment (optical recombination in the K' valley), this requires the final state of X^- to switch valleys depending on the B-field polarity. Because X^- (trion resonance T_1) has wave function contributions from both T_T^{inter} and T_S^{intra} with an electron situated in the lower conduction band c_1 with either spin $\downarrow$ or spin $\uparrow$, the "flavor" of this state is therefore determined by the polarity of the magnetic field, a direct consequence of the quantum superposition of its trion eigenstates at $B = 0$ T. The X^- magneto-optical response directly reflects the properties of both trion configurations at zero magnetic field, while in our experiments, we selectively detect the T_S^{intra} (T_T^{inter}) trion with a spin-$\uparrow$ electron (spin-$\downarrow$ electron) in K' (K) for $B > 0$ ($B < 0$).

We continue to investigate the density dependent X^- valley Zeeman shift $\Delta E_{VZ} = \frac{1}{2} g \mu_B B$ of X^- for positive and negative magnetic field orientations [$g(s^+)$ and $g(s^-)$] at higher densities. The valley Zeeman shift directly encodes spin and orbital properties [8,41–45] and its gate voltage dependence is presented in Fig. 3(d) (for raw data see the Supplemental Material [55], which includes Refs. [51,71]). When the electron density is low, such that only the $\nu = +0$ LL is occupied in c_1, the valley Zeeman shift for positive and negative magnetic fields are equal. However, for densities such that the $\nu = +1$ LL is occupied (n_1), a strong asymmetry emerges in positive and negative magnetic fields. A quantitative description of the trion valley Zeeman shift at fixed density has recently been reported for singlet and triplet trions in WSe_2 [49], consistent with our observations for MoS_2. The asymmetry of the X^- valley Zeeman shift, $\Delta E_{VZ}^{X^-}(n, B) = 1/2(\tau_z g_{X^-} - \tau_e g_e)\mu_B B - g_l(n)\mu_B|B|$, originates in the density-dependent LL occupation, $g_l(n)$ of the final state, with the electron residing in a LL (for details, see the Supplemental Material). For an electron density above $n_1 \sim 3 \times 10^{12}$ cm^{-2}, the combination of spin, valley, and cyclotron energy results in asymmetric LL dispersions in positive and negative magnetic fields for LLs with filling factors $\nu \gtrless +1$. As shown in Fig. 3(d), this manifests itself as asymmetric slopes for positive and negative B-field directions. Since $\Delta E_{\hbar\omega}^{+} + \Delta E_{\hbar\omega}^{-} = -(\hbar\omega_c - \hbar\omega_T)$, we determine the simple equation $\Delta + \frac{1}{m_e} - \frac{1}{m_T} = 0$ with $\Delta = g_{ave}/2 = \frac{1}{2}[g(s^+) + g(s^-)]/2$ and the trion mass $m_T = 2m_e + m_h$, which describes the shift of a trion in a magnetic field (for details on the determination of the electron mass, see the Supplemental Material [55], which includes Refs. [9,49,72]). Considering a hole mass of $m_h = 0.6$ [72], we obtain an electron mass at low electron densities (regime I) of $m_e \sim 0.43$ that is in excellent agreement with literature [see Fig. 3(e)] [23]. For higher voltages (regime II), m_e decreases due to the population of c_1 renormalizing the trion wave function due to many-body effects.

In summary, we have shown that trions in MoS_2 are quantum superpositions of inter- and intravalley spin states for the lowest electron densities close to the trion formation threshold. The observed exchange splitting and binding energies of the different trion species were shown to be strongly sensitive to electron-hole exchange effects. Moreover, pronounced nonuniformity in the Zeeman shift of the intravalley trion revealed the importance of Landau level occupation dependent initial and final state energies. This fully accounts for recently observed variations in the exciton g factor [53]. Our

results expand the current understanding of trion complexes in monolayer MoS_2 and show that their wave functions are strongly admixed, signatures of which are directly encoded in the evolution of valley Zeeman shifts.

This work was supported by Deutsche Forschungsgemeinschaft (DFG) through the TUM International Graduate School of Science and Engineering (IGSSE) and the German Excellence Cluster-MCQST and e-conversion. We gratefully acknowledge financial support by the Ph.D. program ExQM of the Elite Network of Bavaria. We also gratefully acknowledge financial support from the European Union's Horizon 2020 research and innovation programme under Grant Agreement No. 820423 (S2QUIP), the German Federal Ministry of Education and Research via the funding program Photonics Research Germany (Contract No. 13N14846), and the Bavarian Academy of Sciences and Humanities. M.F., A.S., and F.J. were supported by the Deutsche Forschungsgemeinschaft (DFG) within RTG 2247 and through a grant for CPU time at the HLRN (Berlin/Göttingen). J.K. and M.F. acknowledge support by the Alexander von Humboldt Foundation. J.J.F. and A.H. acknowledge support from the Technical University of Munich Institute for Advanced Study, funded by the German Excellence Initiative and the European Union FP7 under Grant Agreement No. 291763 and the German Excellence Strategy Munich Center for Quantum Science and Technology (MCQST). Moreover, J.J.F. gratefully acknowledges the DFG for financial support via FI 947/8-1 and DI 2013/5-1 of SPP-2244. K.W. and T.T. acknowledge support from the Elemental Strategy Initiative conducted by the MEXT, Japan, Grant No. JPMXP0112101001, JSPS KAKENHI Grant No. JP20H00354, and the CREST (JPMJCR15F3), JST. The work has been partially supported by the EC Graphene Flagship project, by the ANR projects ANR-17-CE24-0030 and ANR-19-CE09-0026. M.F., A.S., and F.J. thank G. Schönhoff, M Rösner, and T. Wehling for providing material-realistic band structures and bare as well as screened Coulomb matrix elements.

J.K. and M.F. contributed equally to this work. J.K., A.Hö., A.H., M.P., C.F., J.J.F., and A.V.S. conceived and designed the experiments, A.Hö. and J.K. prepared the samples, K.W. and T.T. provided high-quality hBN bulk crystals, J.K., A.Hö., A.D., C.F., and A.V.S. performed the optical measurements, J.K. and A.V.S. analyzed the data, M.F., A.S., and F.J. computed the trion fine structure, J.K., M.F., A.S., A.V.S, and J.J.F. wrote the manuscript with input from all co-authors.

[1] K. Kheng, R. T. Cox, M. Y. d'Aubigné, F. Bassani, K. Saminadayar, and S. Tatarenko, Phys. Rev. Lett. **71**, 1752 (1993).
[2] G. Finkelstein, H. Shtrikman, and I. Bar-Joseph, Phys. Rev. Lett. **74**, 976 (1995).
[3] H. Buhmann, L. Mansouri, J. Wang, P. H. Beton, N. Mori, L. Eaves, M. Henini, and M. Potemski, Phys. Rev. B **51**, 7969 (1995).
[4] S. Bar-Ad and I. Bar-Joseph, Phys. Rev. Lett. **68**, 349 (1992).
[5] A. Chernikov, T. C. Berkelbach, H. M. Hill, A. Rigosi, Y. Li, O. B. Aslan, D. R. Reichman, M. S. Hybertsen, and T. F. Heinz, Phys. Rev. Lett. **113**, 076802 (2014).
[6] X. Xu, W. Yao, D. Xiao, and T. F. Heinz, Nat. Phys. **10**, 343 (2014).
[7] Z. Wang, K. F. Mak, and J. Shan, Phys. Rev. Lett. **120**, 066402 (2018).
[8] A. V. Stier, K. M. McCreary, B. T. Jonker, J. Kono, and S. A. Crooker, Nat. Commun. **7**, 10643 (2016).
[9] A. V. Stier, N. P. Wilson, K. A. Velizhanin, J. Kono, X. Xu, and S. A. Crooker, Phys. Rev. Lett. **120**, 057405 (2018).
[10] D. Xiao, G.-B. Liu, W. Feng, X. Xu, and W. Yao, Phys. Rev. Lett. **108**, 196802 (2012).
[11] K. F. Mak, K. He, C. Lee, G. H. Lee, J. Hone, T. F. Heinz, and J. Shan, Nat. Mater. **12**, 207 (2013).
[12] J. S. Ross, S. Wu, H. Yu, N. J. Ghimire, A. M. Jones, G. Aivazian, J. Yan, D. G. Mandrus, D. Xiao, W. Yao, and X. Xu, Nat. Commun. **4**, 1474 (2013).
[13] A. Chernikov, A. M. van der Zande, H. M. Hill, A. F. Rigosi, A. Velauthapillai, J. Hone, and T. F. Heinz, Phys. Rev. Lett. **115**, 126802 (2015).
[14] M. Sidler, P. Back, O. Cotlet, A. Srivastava, T. Fink, M. Kroner, E. Demler, and A. Imamoglu, Nat. Phys. **13**, 255 (2017).
[15] M. Barbone, A. R.-P. Montblanch, D. M. Kara, C. Palacios-Berraquero, A. R. Cadore, D. D. Fazio, B. Pingault, E. Mostaani, H. Li, B. Chen, K. Watanabe, T. Taniguchi, S. Tongay, G. Wang, A. C. Ferrari, and M. Atatüre, Nat. Commun. **9**, 3721 (2018).
[16] H. Yu, G.-B. Liu, P. Gong, X. Xu, and W. Yao, Nat. Commun. **5**, 3876 (2014).
[17] A. M. Jones, H. Yu, J. R. Schaibley, J. Yan, D. G. Mandrus, T. Taniguchi, K. Watanabe, H. Dery, W. Yao, and X. Xu, Nat. Phys. **12**, 323 (2016).
[18] G. Plechinger, P. Nagler, A. Arora, R. Schmidt, A. Chernikov, A. G. del Águila, P. C. Christianen, R. Bratschitsch, C. Schüller, and T. Korn, Nat. Commun. **7**, 12715 (2016).
[19] E. Courtade, M. Semina, M. Manca, M. M. Glazov, C. Robert, F. Cadiz, G. Wang, T. Taniguchi, K. Watanabe, M. Pierre, W. Escoffier, E. L. Ivchenko, P. Renucci, X. Marie, T. Amand, and B. Urbaszek, Phys. Rev. B **96**, 085302 (2017).
[20] M. Drüppel, T. Deilmann, P. Krüger, and M. Rohlfing, Nat. Commun. **8**, 2117 (2017).
[21] G. Wang, C. Robert, M. M. Glazov, F. Cadiz, E. Courtade, T. Amand, D. Lagarde, T. Taniguchi, K. Watanabe, B. Urbaszek, and X. Marie, Phys. Rev. Lett. **119**, 047401 (2017).
[22] A. Arora, N. K. Wessling, T. Deilmann, T. Reichenauer, P. Steeger, P. Kossacki, M. Potemski, S. Michaelis de Vasconcellos, M. Rohlfing, and R. Bratschitsch, Phys. Rev. B **101**, 241413 (2020).
[23] A. Kormányos, G. Burkard, M. Gmitra, J. Fabian, V. Zólyomi, N. D. Drummond, and V. Fal'ko, 2D Mater. **2**, 022001 (2015).
[24] Z. Wang, J. Shan, and K. F. Mak, Nat. Nanotechnol. **12**, 144 (2017).

[25] Y. Zhou, G. Scuri, D. S. Wild, A. A. High, A. Dibos, L. A. Jauregui, C. Shu, K. D. Greve, K. Pistunova, A. Y. Joe, T. Taniguchi, K. Watanabe, P. Kim, M. D. Lukin, and H. Park, Nat. Nanotechnol. **12**, 856 (2017).

[26] X.-X. Zhang, T. Cao, Z. Lu, Y.-C. Lin, F. Zhang, Y. Wang, Z. Li, J. C. Hone, J. A. Robinson, D. Smirnov, S. G. Louie, and T. F. Heinz, Nat. Nanotechnol. **12**, 883 (2017).

[27] M. R. Molas, C. Faugeras, A. O. Slobodeniuk, K. Nogajewski, M. Bartos, D. M. Basko, and M. Potemski, 2D Mater. **4**, 021003 (2017).

[28] Z. Lu, D. Rhodes, Z. Li, D. V. Tuan, Y. Jiang, J. Ludwig, Z. Jiang, Z. Lian, S.-F. Shi, J. Hone, H. Dery, and D. Smirnov, 2D Mater. **7**, 015017 (2019).

[29] C. Robert, B. Han, P. Kapuscinski, A. Delhomme, C. Faugeras, T. Amand, M. R. Molas, M. Bartos, K. Watanabe, T. Taniguchi, B. Urbaszek, M. Potemski, and X. Marie, Nat. Commun. **11**, 4037 (2020).

[30] X.-X. Zhang, Y. You, Shu Yang Frank Zhao, and T. F. Heinz, Phys. Rev. Lett. **115**, 257403 (2015).

[31] A. Arora, M. Koperski, K. Nogajewski, J. Marcus, C. Faugeras, and M. Potemski, Nanoscale **7**, 10421 (2015).

[32] G.-B. Liu, W.-Y. Shan, Y. Yao, W. Yao, and D. Xiao, Phys. Rev. B **88**, 085433 (2013).

[33] T. Deilmann and K. S. Thygesen, Phys. Rev. B **96**, 201113(R) (2017).

[34] A. Torche and G. Bester, Phys. Rev. B **100**, 201403(R) (2019).

[35] T. Deilmann, P. Krüger, and M. Rohlfing, Phys. Rev. Lett. **124**, 226402 (2020).

[36] M. Bieniek, L. Szulakowska, and P. Hawrylak, Phys. Rev. B **101**, 125423 (2020).

[37] D. Y. Qiu, T. Cao, and S. G. Louie, Phys. Rev. Lett. **115**, 176801 (2015).

[38] A. Steinhoff, M. Florian, A. Singh, K. Tran, M. Kolarczik, S. Helmrich, A. W. Achtstein, U. Woggon, N. Owschimikow, F. Jahnke, and X. Li, Nat. Phys. **14**, 1199 (2018).

[39] J. Jadczak, J. Kutrowska-Girzycka, M. Bieniek, T. Kazimierczuk, P. Kossacki, J. J. Schindler, J. Debus, K. Watanabe, T. Taniguchi, C. H. Ho, A. Wójs, P. Hawrylak, and L. Bryja, Nanotechnology **32**, 145717 (2021).

[40] M. Grzeszczyk, K. Olkowska-Pucko, K. Watanabe, T. Taniguchi, A. Babiński, and M. R. Molas, Nanoscale **13**, 18726 (2021).

[41] G. Aivazian, Z. Gong, A. M. Jones, R.-L. Chu, J. Yan, D. G. Mandrus, C. Zhang, D. Cobden, W. Yao, and X. Xu, Nat. Phys. **11**, 148 (2015).

[42] A. Srivastava, M. Sidler, A. V. Allain, D. S. Lembke, A. Kis, and A. Imamoğlu, Nat. Phys. **11**, 141 (2015).

[43] D. MacNeill, C. Heikes, K. F. Mak, Z. Anderson, A. Kormányos, V. Zólyomi, J. Park, and D. C. Ralph, Phys. Rev. Lett. **114**, 037401 (2015).

[44] Y. Li, J. Ludwig, T. Low, A. Chernikov, X. Cui, G. Arefe, Y. D. Kim, A. M. van der Zande, A. Rigosi, H. M. Hill, S. H. Kim, J. Hone, Z. Li, D. Smirnov, and T. F. Heinz, Phys. Rev. Lett. **113**, 266804 (2014).

[45] A. V. Stier, N. P. Wilson, G. Clark, X. Xu, and S. A. Crooker, Nano Lett. **16**, 7054 (2016).

[46] A. A. Mitioglu, K. Galkowski, A. Surrente, L. Klopotowski, D. Dumcenco, A. Kis, D. K. Maude, and P. Plochocka, Phys. Rev. B **93**, 165412 (2016).

[47] F. Cadiz, E. Courtade, C. Robert, G. Wang, Y. Shen, H. Cai, T. Taniguchi, K. Watanabe, H. Carrere, D. Lagarde, M. Manca, T. Amand, P. Renucci, S. Tongay, X. Marie, and B. Urbaszek, Phys. Rev. X **7**, 021026 (2017).

[48] T. Smoleński, O. Cotlet, A. Popert, P. Back, Y. Shimazaki, P. Knüppel, N. Dietler, T. Taniguchi, K. Watanabe, M. Kroner, and A. Imamoglu, Phys. Rev. Lett. **123**, 097403 (2019).

[49] T. P. Lyons, S. Dufferwiel, M. Brooks, F. Withers, T. Taniguchi, K. Watanabe, K. S. Novoselov, G. Burkard, and A. I. Tartakovskii, Nat. Commun. **10**, 2330 (2019).

[50] M. Goryca, J. Li, A. V. Stier, T. Taniguchi, K. Watanabe, E. Courtade, S. Shree, C. Robert, B. Urbaszek, X. Marie, and S. A. Crooker, Nat. Commun. **10**, 4172 (2019).

[51] E. Liu, J. van Baren, T. Taniguchi, K. Watanabe, Y.-C. Chang, and C. H. Lui, Phys. Rev. Lett. **124**, 097401 (2020).

[52] T. Wang, Z. Li, Z. Lu, Y. Li, S. Miao, Z. Lian, Y. Meng, M. Blei, T. Taniguchi, K. Watanabe, S. Tongay, W. Yao, D. Smirnov, C. Zhang, and S.-F. Shi, Phys. Rev. X **10**, 021024 (2020).

[53] J. Klein, A. Hötger, M. Florian, A. Steinhoff, A. Delhomme, T. Taniguchi, K. Watanabe, F. Jahnke, A. W. Holleitner, M. Potemski, C. Faugeras, J. J. Finley, and A. V. Stier, Phys. Rev. Research **3**, L022009 (2021).

[54] J. G. Roch, G. Froehlicher, N. Leisgang, P. Makk, K. Watanabe, T. Taniguchi, and R. J. Warburton, Nat. Nanotechnol. **14**, 432 (2019).

[55] See Supplemental Material at http://link.aps.org/supplemental/10.1103/PhysRevB.105.L041302 for description of the field effect device to control the carrier density, theoretical calculations of the trion spectra, extended data on the Landau levels of the negatively charged trion, and the calculation of the density dependent electron mass.

[56] M. Rohlfing and S. G. Louie, Phys. Rev. B **62**, 4927 (2000).

[57] L. J. Sham and T. M. Rice, Phys. Rev. **144**, 708 (1966).

[58] M. M. Denisov and V. P. Makarov, Phys. Status Solidi B **56**, 9 (1973).

[59] A. Esser, R. Zimmermann, and E. Runge, Phys. Status Solidi B **227**, 317 (2001).

[60] M. Florian, M. Hartmann, A. Steinhoff, J. Klein, A. W. Holleitner, J. J. Finley, T. O. Wehling, M. Kaniber, and C. Gies, Nano Lett. **18**, 2725 (2018).

[61] A. Steinhoff, M. Rösner, F. Jahnke, T. O. Wehling, and C. Gies, Nano Lett. **14**, 3743 (2014).

[62] M. Rösner, E. Şaşıoğlu, C. Friedrich, S. Blügel, and T. O. Wehling, Phys. Rev. B **92**, 085102 (2015).

[63] S. Balay, S. Abhyankar, M. Adams, J. Brown, P. Brune, K. Buschelman, L. Dalcin, V. Eijkhout, W. Gropp, D. Kaushik, M. Knepley, L. McInnes, K. Rupp, B. Smith, S. Zampini, H. Zhang, and H. Zhang, PETSc, http://www.mcs.anl.gov/petsc/ (2016).

[64] A. Castellanos-Gomez, M. Buscema, R. Molenaar, V. Singh, L. Janssen, H. S. J. van der Zant, and G. A. Steele, 2D Mater. **1**, 011002 (2014).

[65] J. Wierzbowski, J. Klein, F. Sigger, C. Straubinger, M. Kremser, T. Taniguchi, K. Watanabe, U. Wurstbauer, A. W. Holleitner, M. Kaniber, K. Müller, and J. J. Finley, Sci. Rep. **7**, 12383 (2017).

[66] C. R. Dean, A. F. Young, I. Meric, C. Lee, L. Wang, S. Sorgenfrei, K. Watanabe, T. Taniguchi, P. Kim, K. L. Shepard, and J. Hone, Nat. Nanotechnol. **5**, 722 (2010).

[67] K. K. Kim, A. Hsu, X. Jia, S. M. Kim, Y. Shi, M. Dresselhaus, T. Palacios, and J. Kong, ACS Nano **6**, 8583 (2012).

[68] B. Hunt, J. D. Sanchez-Yamagishi, A. F. Young, M. Yankowitz, B. J. LeRoy, K. Watanabe, T. Taniguchi, P. Moon, M. Koshino, P. Jarillo-Herrero, and R. C. Ashoori, Science **340**, 1427 (2013).

[69] A. Laturia, M. L. V. de Put, and W. G. Vandenberghe, npj 2D Mater. Appl. **2**, 6 (2018).

[70] F. Rose, M. O. Goerbig, and F. Piéchon, Phys. Rev. B **88**, 125438 (2013).

[71] R. Pisoni, A. Kormányos, M. Brooks, Z. Lei, P. Back, M. Eich, H. Overweg, Y. Lee, P. Rickhaus, K. Watanabe, T. Taniguchi, A. Imamoglu, G. Burkard, T. Ihn, and K. Ensslin, Phys. Rev. Lett. **121**, 247701 (2018).

[72] T. Eknapakul, P. D. C. King, M. Asakawa, P. Buaphet, R.-H. He, S.-K. Mo, H. Takagi, K. M. Shen, F. Baumberger, T. Sasagawa, S. Jungthawan, and W. Meevasana, Nano Lett. **14**, 1312 (2014).